S0013-4651(99)01-089-7 CCC: $7.00

In Situ Raman Microscopy of Chromate Effects on Corrosion Pits in Aluminum Alloy

Jeremy D. Ramsey and Richard L. McCreery*

Department of Chemistry, The Ohio State University, Columbus, Ohio 43210, USA

In situ, *ex situ*, and microscopic Raman spectroscopy were used to examine the interactions of dilute chromate solutions with actively corroding pits in aluminum alloy used for aerospace applications (AA-2024-T3). Approximately 10^{-3} M Cr(VI) in salt solution greatly reduces alloy corrosion, and soluble Cr(VI) is a major component of chromate conversion coatings (CCC). The interactions of dilute Cr(VI) with corroding alloy are likely to underlie the "self-healing" property of CCCs which make them so useful. Raman microscopy revealed that 10^{-3} M Cr(VI) was transported into an active pit and formed a chromate corrosion product (CCP) observable by its distinctive ~850 cm^{-1} Raman band. This band was concentrated in pits and difficult to observe on the unpitted surface. Detailed spectroscopy of the CCP and several synthetic analogs revealed that the CCP is a mixed oxide of Al(III) and Cr(VI). Electrostatic bonding between the $Al(OH)_x$ matrix and Cr(VI) is favored when the $Al(OH)_3$ is cationic at low pH, while covalent bonding is also possible at higher pH. The spectra of the CCP formed in AA 2024 pits implies a local pH in the region of 6 to 7. The implications of these findings to the corrosion protection mechanism of Cr(VI) on aluminum are considered.

Manuscript submitted January 25, 1999; revised manuscript received July 8, 1999.

Chromium(VI) oxides are efficient inhibitors of localized corrosion on a variety of metals, particularly aluminum and its alloys. However, the environmental toxicity of Cr(VI) has stimulated the development of a replacement. The use of Cr(VI) is vital to the aerospace industry as aluminum alloys are widely used in aircraft production, but the mechanism of protection by chromate is not fully understood. Aluminum alloy 2024 (AA 2024-T3) is an example of a widely used aircraft alloy comprised of an aluminum matrix and alloying elements Cu (4.4%), Mg (1.5%), and Mn (0.6%). Unfortunately, the alloy has a heterogeneous microstructure that is largely responsible for the susceptibility of the alloy to localized attack.[1,2]

Chromium corrosion coatings (CCC) have been found to be very effective for the protection of AA 2024-T3 from localized corrosion. Of special interest is the possibility of "self-healing" of a CCC after mechanical damage. We demonstrated previously that a scratch or defect in a CCC film can be protected by the migration of soluble Cr(VI) species from a coated sample.[3] Dilute chromate ($<10^{-3}$ M) is sufficient to increase the polarization resistance of AA 2024 alloy by two orders of magnitude after exposure of alloy to chromate solution at open circuit. Structural examination of the CCC film using vibrational spectroscopy shows a reversible binding of Cr(VI) oxides to a Cr(III) oxide matrix allowing the CCC to behave as a store for soluble Cr(VI) inhibitor.[4] These observations support a self-healing mechanism based on storage of Cr(VI) in the CCC, release of dilute Cr(VI) by moisture or mechanical damage, then protection of a scratch or defect by the dilute Cr(VI).

The chemistry of the interaction of dilute Cr(VI) oxides with a scratch or an unprotected alloy is unknown. Theories such as the accumulation of Cr(VI) at active sites[3] and the sealing of anodic films[5-9] are commonly used to explain protection. The interaction of Cr(VI) with anodic films is also not well understood. Many studies on both hydrated alumina films[5-9] and solids[10,11] have been undertaken. Spanos *et al*. have examined chromate adsorption based on chemisorption and physisorption on the surface of hydrated γ-alumina.[11] Examination of anodic films sealed in dichromate solutions show that interactions at pH values below the pH of zero charge result in electrostatic interactions with no major polarization or ligand substitution to the tetrahedral CrO_4 structure.[8] It was also established that the form of the chromium species in the sealed film was predominantly Cr(VI), while air-formed films, which contain many more defects,[12] contain mostly Cr(III).[7]

While Cr(VI) is widely thought to interact preferentially with the aluminum oxide film, there is evidence that a Cr(VI) product is deposited in or around pits on the AA 2024-T3 surface.[3] This product appeared to be similar to a Cr(III)/Cr(VI) mixed oxide and was thought to be due to the accumulation of Cr(VI) in active pits. Experimentally determined pit conditions have shown that inside the pit there are high concentrations of aluminum ion[13] with a moderately acidic pH.[13-15] The pits are believed to electrostatically sorb anions, such as Cr(VI) oxides, from the bulk solution in order to neutralize the accumulated positive charge.

This report is based mainly on Raman spectroscopy of AA 2024-T3 and various chromium and aluminum compounds. Raman spectra are molecular fingerprints which can be used to distinguish specific chemical species. Of direct importance in corrosion systems is the capacity for monitoring samples *in situ*, in air, or in solution; to study dynamic systems on a time scale of a few milliseconds to many days; and to sample specific areas as small as 1-2 μm for sufficiently strong scatterers. Raman spectroscopy without surface enhancement has also been shown to be very sensitive to surface films on solid electrodes with the capability for observing submonolayer surface coverage of organic adsorbates on carbon.[16-19]

The work described herein addresses three objectives related to Cr(VI) actions on AA 2024-T3 alloy. First, *in situ* Raman spectroscopy was used to monitor the transport of chromate species into active pits in the alloy and subsequent formation of a corrosion product. Second, the distribution of this product on the alloy surface was observed with Raman microscopy and imaging. Third, the chemical nature of the corrosion product was examined by comparing its spectra to known, synthetic materials.

Experimental

Reagents.—Reagent grade aluminum nitrate, chromium(III) nitrate, and potassium dichromate were purchased from Alfa Aesar and used as received. All solutions were prepared using "Nanopure" water (Barnstead) with a minimum resistivity of 18 MΩ. Aluminum alloy 2024-T3 samples produced by the Aluminum Company of America were obtained from Joseph T. Ryerson and Son, Inc. All other chemicals were of reagent grade and used as received. Samples of Cr(VI) adsorbed to $Al(OH)_x$ were prepared by adding 2 g of reagent grade $Al(OH)_3$ powder to 75 mL of 0.02 M $K_2Cr_2O_7$. After stirring for 2 h, the solid was collected by filtration, rinsed twice with "Nanopure" water, and the Raman spectra obtained. Al(III)/Cr(VI) mixed oxide was prepared by adding 1 M NaOH solution dropwise to 50 mL of a solution containing 0.2 M $Al(NO_3)_3$ and 0.03 M $K_2Cr_2O_7$. At a pH above about 3, a solid formed which was filtered, rinsed, and dried. The pH at the time of filtering affected the Raman spectrum, as described below.

* Electrochemical Society Active Member.

S0013-4651(99)01-089-7 CCC: $7.00

Alloy sample preparation.—AA 2024-T3 samples were cut into 1 cm^2 squares and mounted in epoxy resin (Buehler). The samples were polished in water with successive grits of silicon carbide polishing paper (240, 400, 600, 800, 1200 grit). Nonaqueous solvents were avoided to prevent Raman interference due to solvent residue.

Pits used in the Raman imaging experiments were generated using both potentiostatic and open-circuit methods. In the open-circuit method, the polished alloy samples were immersed in 0.1 M NaCl solutions for periods of ≥24 h. The samples were then transferred directly into Cr(VI) solutions for 1-24 h and analyzed immediately following treatment. Pits studied with *in situ* Raman experiments were generated using the potentiostatic method. This ensured that the pits were actively corroding and large enough (25-50 μm) for study with this technique. The AA 2024-T3 samples were polarized in aerated 0.1 M NaCl (pH 5) at +150 mV relative to the open-circuit potential. Polarization times varied between 1-15 min depending on the degree of crevice corrosion observed. Following polarization, potential control was removed, and the sample was transferred to the Raman sampling area for analysis. No further potential control was used during the experiment. A magnified surface image was used to select pits exhibiting vigorous hydrogen evolution characteristic of an actively corroding pit. Known volumes of a 0.1 M NaCl/2 mM Cr(VI) solution (pH 4.65) were added, and Raman spectra recorded throughout the duration of the experiment. The size and depth of the pits were not monitored quantitatively during Raman observation, but there did not appear to be any obvious change in pit diameter or depth during the course of spectrum acquisition. The solution depth above the sample was approximately 5 mm. Temperature studies of the surface deposit were performed by placing the treated samples in a furnace with a programmable temperature controller (Eurotherm) for approximately 1 h.

Raman spectroscopy.—All Raman spectra were recorded using a 514.5 nm laser and a charge-coupled device (CCD) detector cooled to < −110°C. Holographic band rejection filters (Kaiser) preceded the entrance slit to the spectrograph for removal of laser light for the *in situ* and microscopic experiments. A few spectra (Fig. 2, 6-8) were obtained with a CdS absorption filter instead of a holographic filter. In these cases, the filter prevented observation of Raman features below 500 cm^{-1}.

Raman microscopic experiments were performed using a Dilor "X-Y" system that has been described earlier.[20] The system consists of an optical microscope (Olympus) mounted at the entrance of the Raman spectrograph. Raman excitation and collection were both performed using a 40 times immersion objective (180° backscattering). The laser spot size focused on the surface was approximately 4-5 μm in diam. To prevent thermal decomposition of the surface deposits due to the high laser power density, the samples were immersed in water during the study. The experimental geometry is described in Fig. 1a.

The *in situ* experiments were performed using a modified Kaiser Holospec Raman spectrograph that has been described previously.[3] A swing mirror and video CCD camera allow the user to locate the incident beam on a pit before Raman analysis. The spatial resolution for this configuration is approximately the diameter of the focused laser spot, or 50 μm. A schematic of the experimental setup is shown in Fig. 1b. Spectra of bulk materials were obtained with a Chromex Raman One spectrometer operating at 514.5 nm.

Electrochemistry.—All electrochemical techniques were performed with a Gamry PC3-300 potentiostat running CMS105 dc corrosion testing software. The experiments used Ag/AgCl reference electrodes (Bioanalytical Systems) with a Pt wire as the counter electrode. All experiments were performed in aerated, unbuffered 0.1 M NaCl adjusted initially to pH 5.

Results

Cr(VI) transport and corrosion product formation.—Figure 2 shows spectra of several reference solutions. The equilibrium between CrO_4^{-2}, $HCrO_4^-$, and $Cr_2O_7^{-2}$ is the subject of some controversy, but is correctly described by several authors,[21,22] based on nuclear magnetic resonance (NMR) and spectrophotometry. At high pH, Cr(VI) is exclusively CrO_4^{-2}, with the Raman spectrum of Fig. 2A. At a pH below the pK_a of $HCrO_4^-$ (~5.8, depending on ionic strength), Cr(VI) is a mixture of $HCrO_4^-$ and $Cr_2O_7^{-2}$, with the dimer favored at high Cr(VI) concentration. For total [Cr(VI)] of 0.1 M, the majority species is $Cr_2O_7^{-2}$, with a Cr(VI)-O frequency of 904 cm^{-1}. At low pH and low total chromate concentration, the Cr(VI) is predominantly $HCrO_4^-$. For example, for a total Cr(VI) concentration of 0.002 M and a pH between 2 and 5, 79% of the Cr(VI) is $HCrO_4^-$, and the remainder is $Cr_2O_7^{-2}$. The 898 cm^{-1} band observed in spectrum 2C is due to $HCrO_4^-$. Although the solution equilibria for Cr(VI) are complex, the Cr(VI) Raman bands in the region 848-904 cm^{-1} are easily distinguished from that of Cr(III) oxide at 550 cm^{-1}. The Raman spectroscopy of the $Cr_2O_7^{-2}$, $HCrO_4^-$, and CrO_4^{-2} system will be discussed in more detail elsewhere.[23]

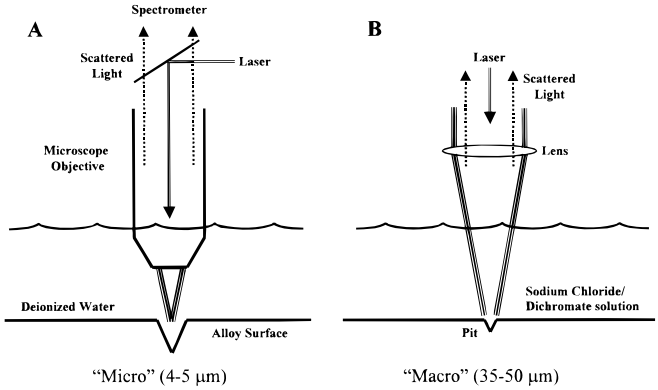

Figure 1. "Micro" mode used a 40 times immersion objective on a Dilor *X*, *Y* imaging Raman spectrometer, and was used for spatially resolved spectra of Fig. 5. "Macro" mode used a 50 mm camera lens and a Kaiser spectrograph. Spectra in Fig. 2, 3, 6, and 8 were obtained with macro mode. Solution depth in both cases was approximately 5 mm.

Using the geometry depicted in Fig. 1B, the Raman spectrum of a pit (diam = ~30 μm) in AA 2024 alloy was monitored before and after Cr(VI) was introduced into the solution. In the spectra of Fig. 3, "0 minutes" is the point immediately after the total Cr(VI) concentration was increased from 0 to 1.6 mM, with vigorous mixing. The short depth of field of the collection optics limits the observation to

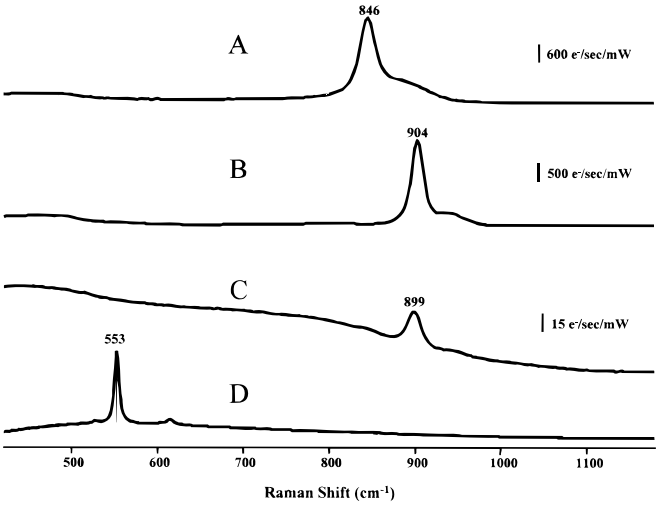

Figure 2. Raman spectra of reagent grade chromium compounds, obtained with macro spectrometer. Intensity scales indicate CCD photoelectrons collected per second of integration time and milliwatts of laser power. (A) 0.1 M K_2CrO_4 solution, pH 9.0; (B) 0.1 M $K_2Cr_2O_7$ solution, pH 3.9; (C) 0.001 M $K_2Cr_2O_7$ solution, pH 4.1; (D) Cr_2O_3 solid as water paste.

S0013-4651(99)01-089-7 CCC: $7.00

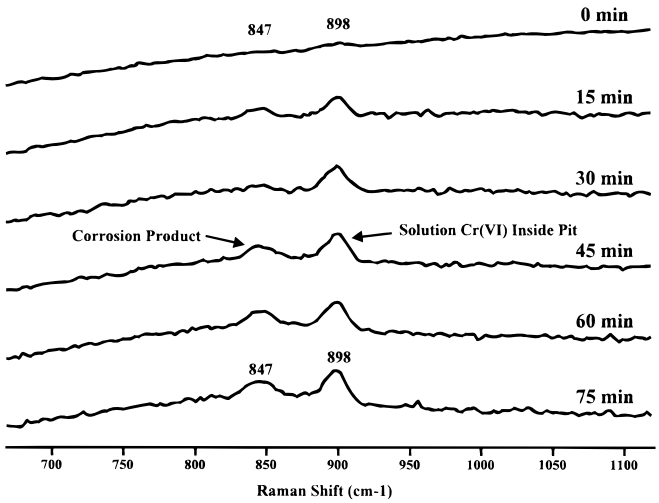

Figure 3. Spectra of a pit in AA 2024-T3 obtained with the apparatus shown in Fig. 1B. At 0 min, the solution Cr(VI) concentration was changed from zero to 1.6 mM, at a pH of 4.7. The short depth of focus of the collection optics suppresses contributions to the spectrum from outside the pit.

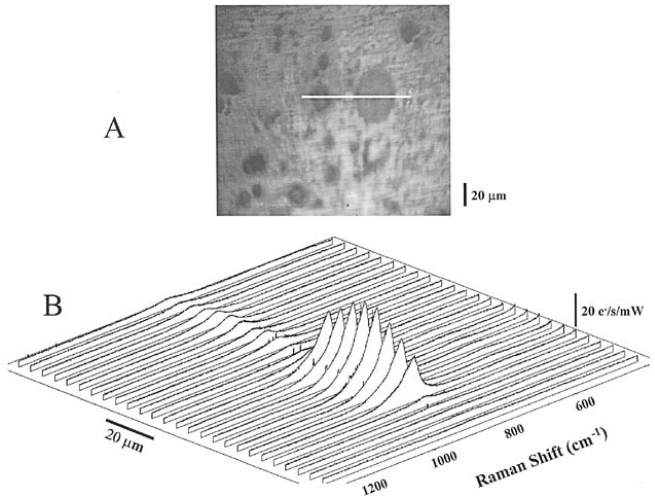

Figure 5. (A) Video micrograph of a AA 2024-T3 surface after 24 h of exposure to 1.6 mM Cr(VI) solution, bulk pH 4.7. (B) 26 Raman spectra obtained at equally spaced intervals along the line in the micrograph, which crosses both a dark and a light pit. *Z* axis is Raman intensity; intensity spikes are due to random interference from background hard radiation.

the immediate region of the pit, so bulk solution species do not contribute significantly to the spectrum. As time progresses, Raman features become visible at 847 and 898 cm^{-1}. As apparent in Fig. 3 and 4, these two bands grow at different times, with the 898 band appearing earlier. The 898 cm^{-1} band was observed in the bulk solution outside the pit, indicating it is due to solution Cr(VI) species, namely, $HCrO_4^-$. The weak Raman intensities cause significant scatter in Fig. 4, but it is clear that the 898 cm^{-1} band initially grows more rapidly than the 847 cm^{-1} band in the region inside the pit. As noted below, the growth of the 898 cm^{-1} band is attributable to diffusion of $HCrO_4^-$ into the pit, while the 847 cm^{-1} band is due to the formation of a corrosion product. The identity and significance of the two features observed in Fig. 3 is discussed further, after additional results on surface chemistry are described.

Spatial distribution of corrosion product.—The spatial distribution of the Raman features apparent in Fig. 3 was determined on the alloy surface using the geometry of Fig. 1A. By moving the sample and the incident laser beam, a map of intensity as a function of position in the x-y plane was constructed.[20] Figure 5 shows a series of 26 spectra obtained along the line indicated in the video micrograph.

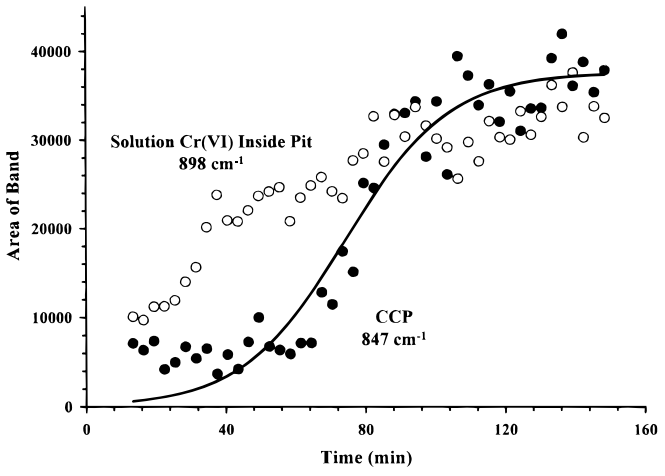

Figure 4. Plots of peak areas of 898 cm^{-1} (open circles) and 847 cm^{-1} (closed circles) Raman bands *vs.* time, for spectra similar to those in Fig. 3. The 847 cm^{-1} feature corresponds to the chromate/$Al(OH)_3$ corrosion product. The solid line is drawn as a visual guide for the closed circles.

The 847 cm^{-1} band intensity is quite low outside pits and varies significantly in different pits. We reported previously[3] that some pits appeared "light" in the video micrograph while others were "dark," and the light pits yielded a stronger Raman intensity. Figure 5A shows a dark pit of about 15 μm diam and a light pit of about 30 μm diam, both of which were on the profile observed with Raman. The more intense 847 cm^{-1} feature apparent in Fig. 5B corresponds to the light pit. As proposed previously, there is a significant concentration of the CCP in the light pit, less in the dark pit, and very little outside the pits.[3] Due to the weak Raman signals, it was not possible to determine CCP distribution within the pit, although such measurements may be possible in the future with different conditions.

Identification of the corrosion product.—Now that the time course and spatial distribution of the 847 cm^{-1} Raman band are known, we turn to the question of the chemical species it represents. Possibilities include Cr(VI) species adsorbed on $Al(OH)_x$, the Cr(VI)/Cr(III) mixed oxide observed in a CCC, a Al(III)/Cr(VI) mixed oxide, or other combinations of Al(III), Cr(III), and Cr(VI). The minor alloy constituents (Cu, Mn, Fe, Mg) could also form corrosion products with chromate, but only the major components were considered here. To provide reference material for comparison, synthetic mixed oxides of Al and Cr were prepared by various routes and their spectra were compared to that of the corrosion product (CCP). These synthetic materials are discussed in turn, and their spectra are presented in Fig. 6.

The top two spectra of Fig. 6 have been discussed in detail elsewhere, and the 858-859 cm^{-1} band has been identified as arising from a Cr(III)/Cr(VI) mixed oxide.[4] Both the CCC (spectrum 6A) and the synthetic oxide (6B) have band shapes and peak positions which differ from those of the corrosion product (6C). The 859 cm^{-1} band does not change peak frequency as the CCC or the Cr(III)/Cr(VI) mixed oxide are heated (Fig. 7) and the frequency is also constant with pH.[4] The corrosion product frequency of 851 cm^{-1} is close to that for synthetic Al(III)/Cr(VI) mixed oxides made by any of three different routes. For example, spectrum 6E is that of reagent grade $Al(OH)_x$ following exposure to 20 mM Cr(VI) solution. The differences in band shape apparent in Fig. 6D and E are due to pH, as shown in Fig. 8. To obtain the materials examined in Fig. 8, $Al(NO_3)_3$ and $K_2Cr_2O_7$ solutions were combined, then the pH was increased with NaOH solution and the precipitate was collected by filtration at the pH values shown. The relative contributions of the 847 and 874 cm^{-1} bands vary with pH, leading to the variation in band shapes. In addition, the Al(III)/Cr(VI) mixed oxide peak fre-

S0013-4651(99)01-089-7 CCC: $7.00

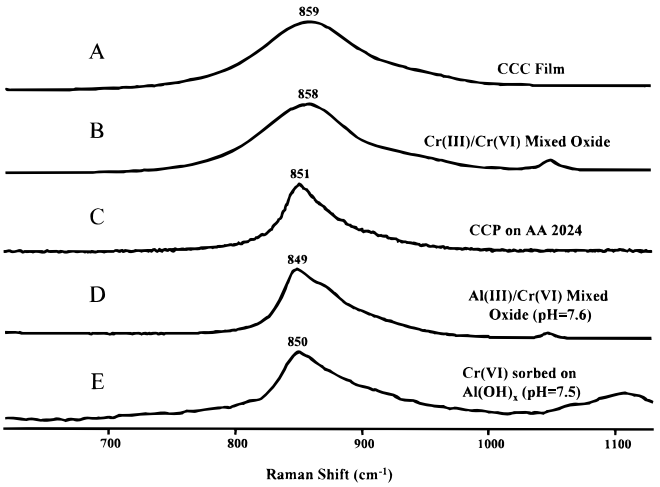

Figure 6. Raman spectra of the 600-1150 cm^{-1} range of CCC, CCP, and synthetic mixed oxides. Small band at 1048 cm^{-1} is due to residual NO_3^- ion. Spectra obtained on wet solids, prepared as described in the Experimental section.

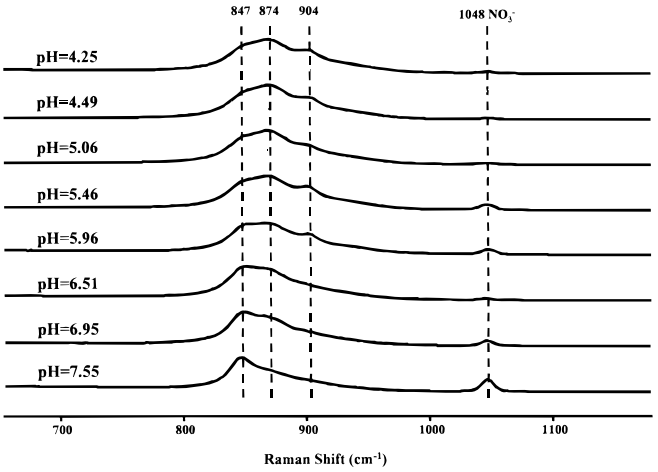

Figure 8. Effect of collection pH on Raman spectra of synthetic Al(III)/Cr(VI) mixed oxides. Precipitates were formed by adding NaOH to Al^{+3} and $Cr_2O_7^{-2}$ solutions, and the solids were collected by filtration at the pH values indicated.

quencies show significant shifts upon heat-treatment, much larger than those observed for the CCC. As shown in Fig. 7, the peak frequencies of the CCP and of Cr(VI) adsorbed on $Al(OH)_x$ shift by 40-50 cm^{-1} while heating to 300°C, while the CCC and Cr(III)/Cr(VI) mixed oxide peak frequencies shift by less than 2 cm^{-1}. The possible subcomponents of the Al(III)/Cr(VI) mixed oxide are currently being investigated, but for the present purposes, it is sufficient to conclude that the products resulting from any of the three synthetic routes are spectroscopically similar, and very different from the Cr(III)/Cr(VI) mixed oxide characterized previously.[4]

There are several immediate structural implications of the results presented in Fig. 6-8. First, the corrosion product which forms when Cr(VI) interacts with a pit in AA 2024 is not spectroscopically identical to the previously characterized 860 cm^{-1} CCC band. The CCP does behave like a Al(III)/Cr(VI) mixed oxide formed from Al(III) hydroxide and soluble Cr(VI). Second, the Al(III)/Cr(VI) mixed oxide spectra of Fig. 8 reveal three bands in the 840-910 cm^{-1} range whose relative intensities vary with pH. The 860 cm^{-1} band observed for the CCC and Cr(III/VI) mixed oxide shows no multiple components or pH variation. Third, the corrosion product spectrum formed when dilute Cr(VI) interacts with a pit in AA 2024-T3 resembles spectra of the Al(III)/Cr(VI) mixed oxide collected in the pH region of 6.9-7.5.

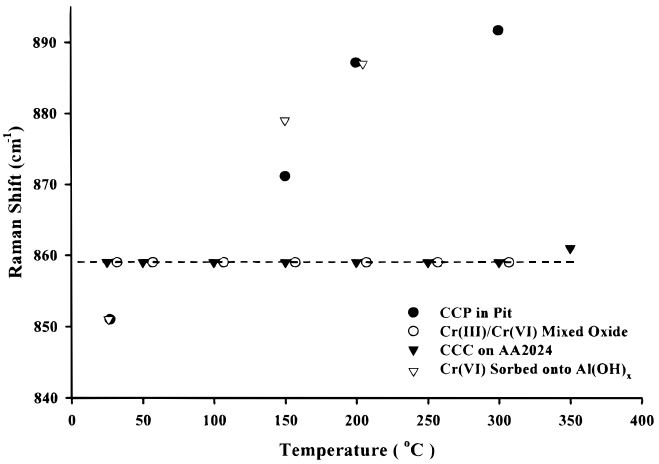

Figure 7. Effect of 1 h heat-treatment on Raman peak frequencies of CCC on AA 2024- T3 on CCC (closed triangle), CCP in AA 2024 pit (closed circles), Cr(III)/Cr(VI) mixed oxide (open circles), and Cr(VI) adsorbed on $Al(OH)_x$ (open triangle).

Discussion

A working model for the self-healing properties of CCC films involves at least three important steps. First, the CCC itself contains a Cr(III)/Cr(VI) mixed oxide which reversibly binds and releases soluble Cr(VI).[4] This oxide has a characteristic 859 cm^{-1} Raman band which is both temperature and pH independent, and which is stable for prolonged periods of time when dry. Second, Cr(VI) may be released into solution (or into a thin film of water), a process which is presumably accelerated by mechanical damage to the CCC. At the low Cr(VI) concentrations expected during this release, most of the Cr(VI) is monomeric, as CrO_4^{-2} or $HCrO_4^-$. Third, this soluble Cr(VI) is transported to a scratch, pit, or defect by diffusion or migration, then provides corrosion protection to the defect.[3] The results of the current investigation are most relevant to the third step, dealing with the interaction of dilute Cr(VI) with corroding AA 2024-T3 alloy.

It is clear from the spectroscopic results in Fig. 6-8 that the corrosion product formed when dilute chromate interacts with a pit is a different compound from the Cr(III)/Cr(VI) mixed oxide in the CCC. Although the CCP and CCC peak frequencies differ by only 10 cm^{-1}, they have very different band structures, temperature dependence, and pH dependence. The CCP has at least three components whose relative concentrations vary with pH, while the CCC exhibits one component in the 800-900 cm^{-1} range under all conditions studied. The CCP band at 850 cm^{-1} is close to that of CrO_4^{-2} in solution (847 cm^{-1}), but has a different band shape. CrO_4^{-2}, $HCrO_4^-$, and $Cr_2O_7^{-2}$ in bulk solution do not show the three component band of Fig. 8 at any pH or concentration examined. Furthermore, the CCP band is not "washed off" by water. In order for the 847 and 898 cm^{-1} bands in Fig. 3 to be due to aqueous CrO_4^{-2} and $HCrO_4^-$, respectively, a fortuitous pH of about 6 is required, and both bands should be removed by rinsing in water. The presence of the 898 cm^{-1} band of $HCrO_4^-$ in the pit indicates a pH unfavorable for CrO_4^{-2} in solution, and the persistence of the 847 cm^{-1} band in Fig. 3 upon rinsing argues strongly against its assignment as CrO_4^{-2} in solution. Furthermore, the absence of an observable 859 cm^{-1} band in Fig. 3 implies that relatively little Cr(III)/Cr(VI) mixed oxide is formed. Since Cr(III) is a relatively weak Raman scatterer under the conditions employed, reduction of Cr(VI) to Cr(III) in or near the pit cannot be ruled out.

The use of chromium oxide supported on alumina as a dehydrogenation catalyst has stimulated significant research on the interac-

S0013-4651(99)01-089-7 CCC: $7.00

tion of chromates with alumina and aluminum hydroxide.[24] Cr(VI) adsorbs on hydrated alumina in aqueous solution by both electrostatic and covalent bonding. In the pH range 6.1-7.5, an Al(III)-O-Cr(VI) covalent bond is formed by a reaction of CrO_4^{-2} or $HCrO_4^-$ with an Al-OH group.[11] At lower pH, the alumina surface becomes cationic due to protonation, and electrostatic binding of anionic chromate species with Al-OH_2^+ group may occur. Unfortunately, there is a large number of possibilities for the structures of species resulting from Cr(VI) adsorption on hydrated alumina, and their relative populations depend strongly on pH and Cr(VI)/Al(III) ratios. The 847 and 874 cm^{-1} bands apparent in Fig. 8 are attributable to two of the possible combinations of Cr(VI) and Al(III) hydroxide. Since the 847 cm^{-1} band increases in relative intensity at higher pH, it may be due to sorbed CrO_4^{-2}. Spanos *et al*. concluded that covalent bonding of Cr(VI) to $Al(OH)_x$ is prevalent above pH ~6.5, due to the significant decrease in surface cationic charge.[11] As the pH is decreased, the 874 cm^{-1} band becomes more prominent, implying that it may be due to sorbed $HCrO_4^-$. Given the many possibilities, it is difficult to assign the 847 and 874 cm^{-1} bands to specific structures. However, it is clear that they result from Cr(VI) sorbed on Al(III) hydroxide, via either electrostatic or covalent interactions.

The concentration of CCP in the pits evident in Fig. 5 is presumably due to the relatively high abundance of $Al(OH)_x$, providing a site for Cr(VI) adsorption. Since Al^{+3} is forming and hydrolyzing to $Al(OH)_x$ in an active pit, there will be a high local surface area of $Al(OH)_x$ available for Cr(VI) adsorption. It is certainly possible that Cr(VI) is adsorbing to the matrix outside pits, but the resulting concentration is near the Raman detection limit.

As noted earlier, the spectroscopic evidence indicates that little Cr(III)/Cr(VI) mixed oxide is formed when chromium(VI) oxide interacts with an active pit. The question arises of why the Cr(VI)/Cr(III) mixed oxide forms rapidly during CCC formation, while dilute chromate leads to an Al(III)/Cr(VI) mixed oxide on a corroding alloy surface. Either the Cr(VI) is not reduced to Cr(III) in the pit, or it is reduced but does not progress to form the Cr(III)/Cr(VI) mixed oxide. The formation conditions of the CCC and the CCP are quite different, and explain the difference in products. The "coating" environment during CCC formation is high in Cr(VI) (~40 mM) and F^- (~14 mM), low in pH (<2), and contains an "accelerator" to catalyze Cr(III) production. In a "field" environment more similar to that studied here, fluoride is absent, there is no accelerator, and Cr(VI) is low (<1 mM). The observations indicate that coating conditions favor Cr(III)/Cr(IV) mixed oxide formation (with its 859 cm^{-1} band), while field conditions favor Al(III)/Cr(VI) oxide formation.

It is quite likely that Cr(VI) is reduced near or in pits, but the resulting Cr(III) does not progress to a Cr(III) hydroxide. The initial Cr(III) species present after reduction are in monomeric form [Cr^{+3}, $Cr(OH)^{2+}$, etc.] and react through intermolecular reactions to form a dimer and higher oligomers.[27,28] Since this mechanism requires aggregation of at least two of the monomer species, the rate law for the overall conversion of the monomeric species to the dimer is at minimum second order. For the Cr(III) hydrolysis reaction, the rate law has been determined, with the reaction being second order in monomer concentration.[25] For example, to accomplish 10% conversion of $Cr(OH)^{2+}$ to the doubly bridged dimer, $Cr_2(\mu\text{-}OH)_2(H_2O)_8^{4+}$, requires a few seconds when the initial concentration of Cr(III) is 40 mM. For 0.1 mM $Cr(OH)_2^+$, the reaction time increases to 9 min.

Under coating conditions, the rapid reduction of Cr(VI) at the exposed aluminum surface produces a large concentration of Cr(III) resulting in a rapid formation of polymeric Cr(III) hydroxides and CCC film formation. The field conditions have low concentrations of Cr(VI) inside the pits and conversely low [Cr(III)], resulting in slow kinetics for the formation of a Cr(III) film. The coating environment also stipulates the presence of fluoride and a reduction accelerator. The fluoride acts as a strong chelating agent of the Al(III) ion and inhibits the formation of the aluminum hydroxide film. AlF_6^{-3} is soluble and has a high formation constant (10^{20}), so little formation of aluminum hydroxide is expected. This accounts for the low concentration of aluminum that is observed in CCC films. A reduction accelerator such as $Fe(CN)_6^{-3}$ acts as a mediator for the reduction of Cr(VI) on the surface of AA 2024-T3.[26] The presence of the accelerator is necessary for fast and thick film formation. With the lack of an accelerator, the Cr(VI) reduction rate is slow, further lowering the concentration of Cr(III) at the alloy surface. Under the field conditions, the formation of a Cr(III)/Cr(VI) mixed oxide is severely hindered, thus allowing the precipitation of an Al(III)/Cr(VI) mixed oxide. The contrast of these environmental conditions and their effect on their chemical behavior is presented in Fig. 9.

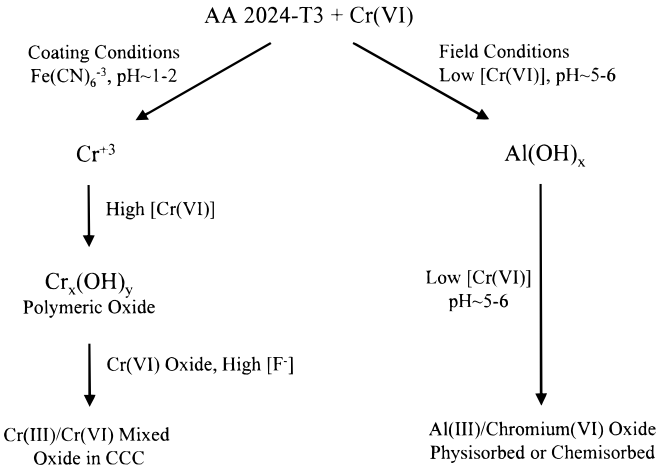

Figure 9. Summary of the formation process for Cr(III)/Cr(VI) mixed oxide in a CCC under coating conditions and Al(III)/Cr(VI) mixed oxide in field conditions.

The conclusion that Cr(VI) forms a physisorbed or chemisorbed mixed oxide with $Al(OH)_x$ in pits does not directly address the question of how chromate protects AA 2024-T3 in the field. However, the results presented here have several implications which may bear on possible anticorrosion mechanisms. First, Cr(VI) adsorption will partially neutralize the cation charge present on alumina in mildly acidic pH.[29,30] This reduction in surface charge may reduce chloride adsorption and possibly stabilize the oxide film. Second, Cr(VI) reduction to Cr(III) requires hydrogen ions, and should increase the local pH (reaction 1)

$$HCrO_4^- + 3e^- + 4H^+ \rightarrow Cr(OH)_3 + H_2O \qquad [1]$$

Comparison of the CCP spectrum with those of Fig. 8 implies that the pit pH is 6 to 7 at the time of CCP formation, significantly higher than that expected from Al^{+3} hydrolysis. This increase in pH may decrease the rate of Al dissolution. It is quite possible that the pH within the pit was lower than 6 during pit growth, but the current results imply that it was between 6 and 7 during CCP formation. Third, the CCP could act as a secondary storage site for Cr(VI). Like the Cr(III)/Cr(VI) mixed oxide in the CCC itself, the Al(III)/Cr(VI) oxide should be able to release Cr(VI) back into solution. Whatever the mechanism of Cr(VI) protection, adsorption to $Al(OH)_x$ in pits (or elsewhere) might prevent loss of Cr(VI) from the coating. Fourth, the process of sealing of oxide films on anodized metals[5-9] may involve an adsorption mechanism similar to that underlying CCP adsorption. The resulting neutralization of the surface charge may protect by reducing chloride adsorption.

On the other hand, protection by Cr(VI) may be unrelated to its behavior in active pits. If the primary protection mechanism is inhibition of oxygen reduction, the cathodic sites may be localized on intermetallic compounds. It is quite possible that Cr(VI) adsorbs to the matrix outside of pits, perhaps specifically at intermetallic particles, but the resulting product is present at levels near or below the Raman detection limit. It is also possible that Cr(VI) is reduced to Cr(III) in the pit and/or on the matrix, in which case Cr(III) might be the cathodic inhibitor.

S0013-4651(99)01-089-7 CCC: $7.00

Summary

Figure 9 incorporates the principal conclusions of the current work. Namely, dilute Cr(VI) is transported into pits in AA-2024-T3 by diffusion and/or migration, where it adsorbs to $Al(OH)_x$ via electrostatic or covalent binding. The resulting mixed oxide product is chemically distinct from the Cr(III)/Cr(VI) mixed oxide formed in a CCC, and a measurable concentration of the Cr(III)/Cr(VI) oxide was not observed. Binding of Cr(VI) to $Al(OH)_x$ reduces the surface charge due to neutralization of cationic sites on the $Al(OH)_x$. The resulting Al(III)/Cr(VI) mixed oxide may effect corrosion protection via several mechanisms, including surface-charge neutralization, displacement of chloride ion, an increase of local pH, or interactions with intermetallic compounds.

Acknowledgments

This work was supported by the U.S. Air Force Office of Scientific Research, contract no. F49620-96-1-0479. The authors wish to thank Gerald Frankel, Martin Kendig, and Lin Xia for useful comments during the research.

The Ohio State University assisted in meeting the publication costs of this article.

References

1. R. G. Buchheit, R. P. Grant, P. F. Hlara, B. McKenzie, and G. L. Zender, *J. Electrochem. Soc.*, **144**, 2621 (1997).
2. G. S. Chen, M. Gao, and R. P. Wei, *Corrosion*, **52**, 8 (1996).
3. J. Zhao, G. Frankel, and R. L. McCreery, *J. Electrochem. Soc.*, **145**, 2258 (1998).
4. L. Xia and R. L. McCreery, *J. Electrochem. Soc.*, **145**, 3083 (1998).
5. M. F. Abd Rabbo, J. A. Richardson, G. C. Wood, and C. K. Jackson, *Corros. Sci.*, **16**, 677 (1976).
6. H. Konno, S. Kobayashi, H. Takahashi, and M. Ngayama, *Corros. Sci.*, **22**, 913 (1982).
7. J. K. Hawkins, H. S. Isaacs, S. M. Heald, J. Tranquada, J. E. Thompson, and G. C. Wood, *Corros. Sci.*, **27**, 391 (1987).
8. J. S. Wainright, O. J. Murphy, and M. R. Antonio, *Corros. Sci.*, **33**, 281 (1992).
9. C. B. Breslin, G. Treacy, and W. M. Caroll, *Corros. Sci.*, **36**, 1143 (1994).
10. R. A. Griffin, A. K. Au, and R. R. Frost, *J. Environ. Sci. Health*, **A12**, 431 (1977).
11. N. Spanos, S. Slavov, C. Kordulis, and A. Lycourghotis, *Langmuir*, **10**, 3134 (1994).
12. J. A. Richardson, G. C. Wood, and W. H. Sutton, *Thin Solid Films*, **16**, 99 (1973).
13. A. Turnbull, *Corros. Sci.*, **23**, 833 (1983).
14. N. J. H. Holroyd, G. M. Scamans, and R. Hermann, in *Corrosion Chemistry Within Pits, Crevices, and Cracks*, A. Turnbull, Editor, p. 495, HMSO Publications, London (1987).
15. K. P. Wong and R. C. Alkire, *J. Electrochem. Soc.*, **137**, 3010 (1990).
16. M. R. Kagan and R. L. McCreery, *Anal. Chem.*, **66**, 4159 (1994).
17. M. A. Fryling, J. Zhao, and R. L. McCreery, *Anal. Chem.*, **67**, 967 (1995).
18. M. R. Kagan and R. L. McCreery, *Langmuir*, **11**, 4041 (1995).
19. Y. C. Liu and R. L. McCreery, *J. Am. Chem. Soc.*, **117**, 11254 (1995).
20. K. Ray and R. L. McCreery, *Anal. Chem.*, **69**, 4680 (1997).
21. N. E. Brasch, D. A. Buckingham, A. B. Evans, and C. R. Clark, *J. Am. Chem. Soc.*, **118**, 7969 (1996).
22. J. J. Cruywagen, J. B. B. Heyns, and E. A. Rohwer, *Polyhedron*, **17**, 1741 (1998).
23. J. D. Ramsey, L. Xia, R. L. McCreery, and M. W. Kendig, *J. Electrochem. Soc.*, In preparation.
24. B. M. Weckhuysen, I. E. Wachs, and R. A. Schoonheydt, *Chem. Rev.*, **96**, 3327 (1996).
25. F. P. Rotzinger, H. Stünzi, and W. Marty, *Inorg. Chem.*, **25**, 489 (1986).
26. L. Xia and R. L. McCreery, *J. Electrochem. Soc.*, **146**, 3083 (1999).
27. H. Stünzi and W. Marty, *Inorg. Chem.*, **22**, 2145 (1983).
28. H. Stünzi, L. Spiccia, F. Rotzinger, and W. Marty, *Inorg. Chem.*, **28**, 66 (1989).
29. N. Sato, *Corrosion*, **5**, 354 (1989).
30. E. McCafferty, *Corros. Sci.*, **371**, 481 (1995).